



ELSEVIER

Available online at www.sciencedirect.com

SCIENCE @ DIRECT®

NDT&E International 36 (2003) 609–617

NDT&E
international

www.elsevier.com/locate/ndteint

Image acquisition techniques for automatic visual inspection of metallic surfaces

Franz Pernkopf^{a,*}, Paul O'Leary^{b,1}

^a*Institute of Communications and Wave Propagation, Graz University of Technology, Graz 8010, Austria*

^b*Institute of Automation, Christian Doppler Laboratory for Sensor and Measurement Systems, University of Leoben, Leoben 8700, Austria*

Received 25 April 2003; revised 16 June 2003; accepted 22 June 2003

Abstract

This paper provides an overview of three different image acquisition approaches for automatic visual inspection of metallic surfaces. The first method is concerned with gray-level intensity imaging, whereby the most commonly employed lighting techniques are surveyed. Subsequently, two range imaging techniques are introduced which may succeed in contrast to intensity imaging if the reflection property across the intact surface changes. However, range imaging for surface inspection is restricted to surface defects with three-dimensional characteristics, e.g. cavities. One range imaging approach is based on light sectioning in conjunction with fast imaging sensors. The second introduced range imaging technique is photometric stereo.

© 2003 Elsevier Ltd. All rights reserved.

Keywords: Surface inspection; Imaging techniques; Range imaging; Light sectioning; Photometric stereo

1. Introduction

Image processing techniques play a crucial role in the growing field of automatic surface inspection. The customer demands are well-founded on the high costs of poor quality in manufacturing, with the resulting costs for correction. Newman and Jain [1] defined the task of inspection as follows: *Inspection is the process of determining if a product deviates from a given set of specifications.*

This paper surveys imaging techniques with their optical arrangements for acquisition of an image of a metallic objects surface for inspection applications. The most practical imaging techniques are discussed with particular emphasis to their applicability and bottlenecks. The choice of the imaging technique is strongly connected to the characteristics of the flaws, the nature of the surface, e.g. shiny machined surfaces versus inhomogeneous scale-covered surfaces, and the required spatial resolution.

Two areas of research which attract the most attention in the literature are considered for the acquisition of the surface image of metallic objects:

- Intensity imaging.
- Range imaging methods which are subdivided into light sectioning techniques and photometric stereo methods.

Before each of these areas is discussed an overview of the literature on surface inspection of steel products is given. Due to the fact that the huge variety of different systems available would lead beyond the scope of this paper, only the most interesting approaches are surveyed. Fernandes et al. [2] proposed a system for the continuous inspection of cast aluminium, where up to 15 different types of defects have to be detected and classified. Vascotto [3] presented a high-speed surface defect identification system for steel strips. Defects with a size of less than 1 mm are detected on a 1300 mm wide strip moving at a maximum speed of 4 m/s. This system is based on a bright and dark field inspection configuration. Stefani et al. [4] demonstrated an industrial inspection arrangement for inspection of continuously extruded cylindrical products which effectively detected defects at a speed up to 10 m/s. Pernkopf and O'Leary [5] presented an approach for inspection of machined high-precision surfaces such as bearing rolls. Only few inspection systems based on range imaging are reported in the literature [6,7]. A survey is given in Newman et al. [1].

* Corresponding author. Tel.: +43-316-873-4436.

E-mail address: pernkopf@inw.tugraz.at (F. Pernkopf).

¹ Tel. : + 43-3842-402-9031.

2. Intensity imaging

Several inspection systems have been presented which are based on gray-level intensity data for inspection [1]. The reflected light collected by the camera sensor forming the intensity image depends on the reflection properties of the surface and the chosen illumination setup. The lighting system is a critical point of intensity imaging of metallic surfaces. The light needs to be provided in a controlled manner to accentuate the desired features of the surface. Designing the optimal lighting setup is one of the most difficult parts of a surface inspection system, which requires a lot of intuition and experiments. There are a rich variety of lighting techniques that may be used for intensity imaging in machine vision. They can be summarized into three general categories:

- *Front lighting.*
- *Back lighting.* This technique is normally used for viewing the silhouette of opaque objects or for inspecting transparent objects.
- *Structured lighting.* This method is used to acquire the three-dimensional shape of an object [8].

For the intensity imaging of metallic surfaces mainly front lighting is relevant and consequently the focus is drawn on this lighting method. Another important distinction is that the front light may be diffused or directional bright field, and dark field. Diffuse front lighting achieves non-directional, uniform illumination, resulting in an image with few shadows or highlights. In practice, the design of a diffuse light source may be difficult due to the fact that the incident light rays should comprise a large range of angles. Nayar et al. [9] show an approach of an extended light source resulting in an increased diffuse reflection component compared to the specular component. Thus, diffuse illumination of specular reflecting surfaces enables an attenuation of the specular component. But diffuse light may also produce non-distinct edges and low contrast on some surfaces. Hence, this type of illumination is suitable for scenes where the contrast between different surface qualities is high.

A sketch of directional bright field and dark field illumination is given in Fig. 1.

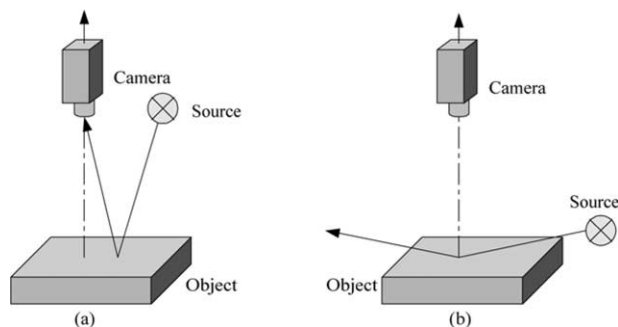


Fig. 1. Front lighting: (a) Bright field illumination, (b) Dark field illumination.

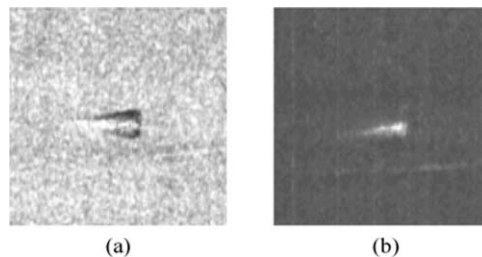


Fig. 2. Intensity image of a planar surface patch with a cavity using directional bright field and dark field lighting: (a) Bright field illumination, (b) Dark field illumination.

In bright field illumination the sensor captures most of the directly reflected light. Thereby, the lighting direction is approximately perpendicular to the inspected surface. The surface appears bright, whereby the features show as a continuum of gray levels.

In dark field illumination the angle of the incident light rays to the surface normal vector is very large. This results in a dark appearance of the surface, but salient features, such as scratches, appear bright in the image.

Selecting between bright field and dark field illumination can enhance or hide surface qualities. Fig. 2 shows an intensity image of a planar surface patch with a cavity using directional bright field and dark field lighting. In the dark field illumination (Fig. 2b) the surface texture has vanished completely.

3. Range imaging

For many inspection applications of metallic surfaces, an acceptable intensity image cannot be produced neither with bright field or dark field lighting nor with diffuse illumination. This is the case if the reflection property across the intact surface changes and the defects may not be emphasized relative to their background using intensity imaging. Surface defects with three-dimensional characteristic, e.g. cavities, scratches, nicks, are visualized with a higher contrast by means of range imaging. A range image depicts the height information of the observed scene. One advantage of range imaging is that surface height information is represented explicitly which is less influenced by a change in the reflection factor across the surface. Range imaging is not competitive to intensity imaging with respect to spatial resolution and acquisition speed. There is an additional step necessary for recovering the depth data from the intensity images.

3.1. Light sectioning

The light sectioning method is a well-known measurement technique for optical determination of object sections. A light plane is projected onto the object from one direction. Most commonly a laser serves as light source. The profile emerging on the scene is viewed from a different direction

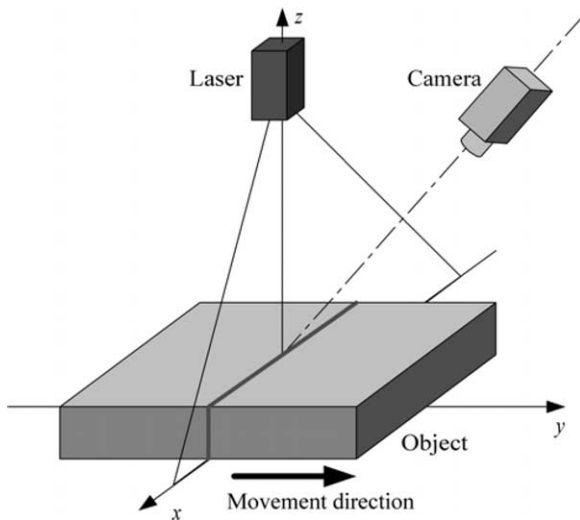


Fig. 3. Principle of light sectioning.

using a camera. Through the known arrangement of the laser light source and the camera the height information of the object can be determined at each point along the profile. The three-dimensional model is gathered by moving the object in one direction while its cross-section is scanned in a sequential manner. The principle of light sectioning is shown in Fig. 3.

One of the drawbacks of this technique is that for each section, first an intensity image with the contour has to be acquired (Fig. 4). Once the profile has been extracted by means of a line detection algorithm [10,11], the line data is converted to range data using the system geometry. Since the profiles are gained sequentially from the intensity

images light sectioning is time consuming. However, fast sensors which deliver several thousand sections per second with a lateral resolution of, e.g. 512 pixels are available [12]. A more detailed introduction into light-sectioning can be found in Refs. [13,14].

Fig. 4 shows a small nick embedded in the edge of a steel block. The contour is extracted from the intensity image consecutively along the edge of the steel block. These profiles are combined to form the spatial geometry of the inspected object.

3.1.1. Equations for the measuring range

The geometric setup for the light sectioning is shown in Fig. 5.

The range r as a function of the arrangement of the camera sensor and the laser is given in Eq. (1), where the sensor plane is assumed to be perpendicular to the optical axis of the camera ($\beta = 0$)

$$r = \frac{B(b_0 \tan \alpha - s) \cos \alpha}{\frac{b_0}{\cos \alpha} - (b_0 \tan \alpha - s) \sin \alpha} = B \frac{b_0 \tan \alpha - s}{b_0 + s \tan \alpha} \quad (1)$$

The symbol b_0 depicts the distance from the optical center to the center of the sensor plane, B is the baseline and s gives the position of light impact on the sensor. This equation is non-linear which means that a constant change Δs across the sensor is associated with a variable change of the measured range Δr . The maximal measuring range interval R_T for a particular setup can be determined by inserting in Eq. (1) the physical dimensions s of the sensor chip (extreme values)

$$s = \pm \frac{N\Delta x}{2}, \quad (2)$$

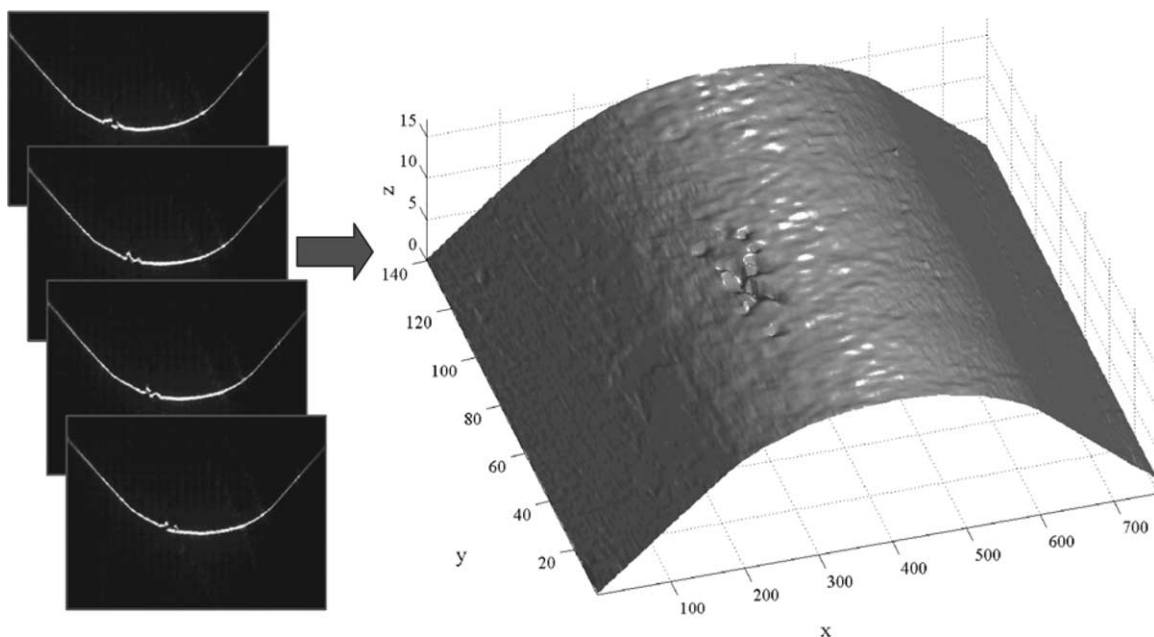


Fig. 4. Geometry of steel block with embedded nick.

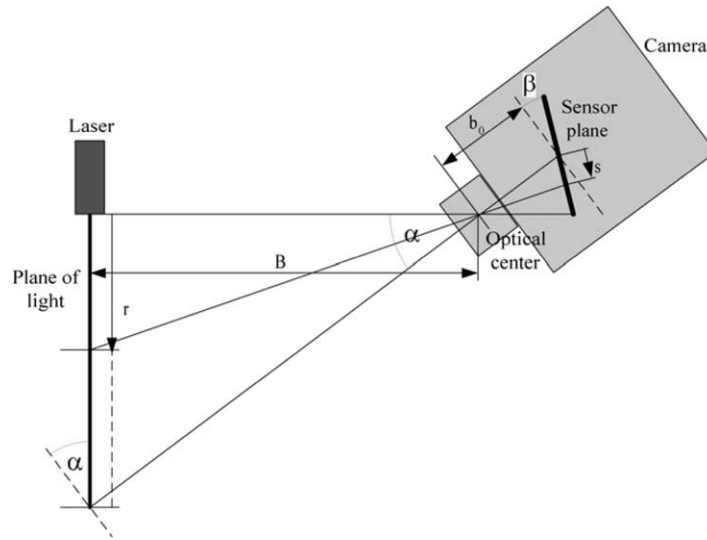


Fig. 5. Geometric setup of light sectioning.

where N is the number of pixels in vertical direction and Δx is the corresponding dimension of one pixel. The range interval R_T after simplification is

$$R_T = \frac{4Bb_0N\Delta x(1+(\tan\alpha)^2)}{4b_0^2-(N\Delta x\tan\alpha)^2} \approx \frac{4BfN\Delta x(1+(\tan\alpha)^2)}{4f^2-(N\Delta x\tan\alpha)^2}, \quad (3)$$

where f denotes the focal length. This equation is useful to determine the range interval of a given setup, or to redesign a system by changing the parameters.

3.1.2. Equations for the width

The geometry for the width is shown in Fig. 6.

The relation between the sensor coordinate t and the world coordinate x can be expressed in the following way

$$x = -\frac{at}{b}. \quad (4)$$

According to Johannesson [14], x in Eq. (4) can be expressed by the setup parameters of the system as

$$x = \frac{-tB}{b_0 \cos \alpha + s \sin \alpha} \quad (5)$$

for the case where the sensor plane is perpendicular to the optical axis of the camera ($\beta = 0$).

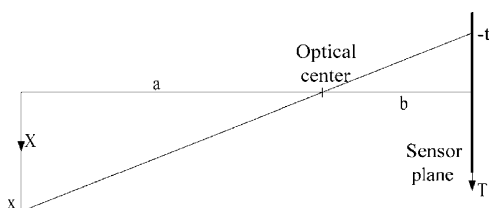


Fig. 6. Geometry of the width.

As shown above (Eqs. (1) and (5)), the range r and the width x can be determined from the sensor offset position s and t by means of the system parameters.

3.1.3. Occlusion

Johannesson [14] addresses the problem of occlusion (Fig. 7) as one of the major problems of light sectioning methods. Either an occlusion is induced by the laser so that no contour line is projected on the area viewed with the camera (laser occlusion) or the camera is not able to visualize the area illuminated by the laser (camera occlusion). In order to minimize the laser and camera occlusion careful considerations about the placement of the laser and the camera are necessary. As shown in Fig. 7 laser occlusion is prevented if the optical center of the camera is more close to the viewed scene than the optical center of the laser. One approach to overcome occlusions is using multiple laser sources and camera sensors.

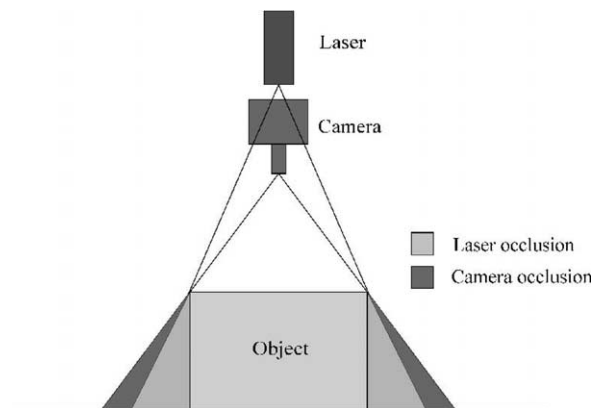


Fig. 7. Laser and camera occlusion.

3.2. Photometric stereo

Photometric stereo refers to an indirect method of range imaging, since the shape of the object is obtained by analysis of the image irradiance of a set of images. In the last few years, this technique achieved increased influence in industrial surface inspection, e.g. Smith and Stamp [15] used photometric stereo for automatic inspection of ceramic tiles. Originally, this technique was developed by Woodham [16]. The idea of photometric stereo is to take several images of a static scene from the same viewpoint, while alternating the illumination direction. This means, that a particular pixel in each of the consecutively acquired images corresponds to the same object point. On the basis of shading caused by the shape of the object in the acquired intensity images the geometry is reconstructed. There exist three degrees of freedom (unknowns) in any particular surface location, the surface reflectance factor (surface albedo), and two degrees of freedom specifying the surface orientation. Consequently, using three images acquired from three different lighting configurations enables the computation of the surface orientation together with its reflectance factor. The principle of photometric stereo is shown in Fig. 8. Normally, white light is utilized but also acquisition of the images in parallel using a color camera and colored light is feasible.

There is a list of possible constraints [8] of this technique, where most of them are uncritical. Among other restrictions, photometric stereo assumes a diffusely reflecting surface characteristic (Lambertian surfaces), an orthographic projection of the three-dimensional object onto the camera sensor, and a parallel illumination. The assumed Lambertian reflectance function is not that restrictive [15], since specular reflecting surfaces approximately show a Lambertian reflection behavior outside the specular region when illuminated with a point light source.

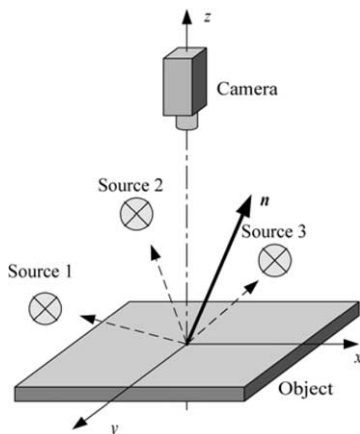


Fig. 8. Principle of photometric stereo.

The following mathematical equations are expressed for 1 pixel. The intensity value of a pixel in the image

$$I(x, y) = R \cos \angle(\mathbf{s}, \mathbf{n}) = R \frac{\mathbf{s}^T \mathbf{n}}{\|\mathbf{s}\| \|\mathbf{n}\|} \quad (6)$$

is computed by the illumination source direction $\mathbf{s} = [s_x \ s_y \ s_z]^T$, the surface normal vector $\mathbf{n} = [n_x \ n_y \ n_z]^T$, and the albedo (surface reflectance factor) R^2 ($\|\mathbf{s}\|$ denotes the magnitude of vector \mathbf{s}). The vectors \mathbf{s} and \mathbf{n} are assumed to have unit length, and the imaging equation simplifies to

$$I(x, y) = R \mathbf{s}^T \mathbf{n}, \quad (7)$$

where $I(x, y)$ and \mathbf{s} are known. To recover R and \mathbf{n} a minimum of three images of a static scene illuminated from different directions is necessary. Let

$$\mathbf{I} = \begin{bmatrix} I_1 \\ I_2 \\ I_3 \end{bmatrix} \quad (8)$$

be the column vector of the intensity values at a point (x, y) for each of three different illumination directions. Further, the illumination directions

$$\mathbf{S} = \begin{bmatrix} s_x^1 & s_y^1 & s_z^1 \\ s_x^2 & s_y^2 & s_z^2 \\ s_x^3 & s_y^3 & s_z^3 \end{bmatrix} \quad (9)$$

are given, where s_x , s_y , and s_z denote the components of \mathbf{s} in the coordinate frame (Fig. 8). The superscript of s refers to the light source 1, 2, or 3. A set of equations can be formed which is solved for \mathbf{n} and R

$$\mathbf{I} = \begin{bmatrix} I_1 \\ I_2 \\ I_3 \end{bmatrix} = R \begin{bmatrix} s_x^1 & s_y^1 & s_z^1 \\ s_x^2 & s_y^2 & s_z^2 \\ s_x^3 & s_y^3 & s_z^3 \end{bmatrix} \begin{bmatrix} n_x \\ n_y \\ n_z \end{bmatrix} = R \mathbf{S} \mathbf{n}. \quad (10)$$

To solve for the reflectance factor R , Eq. (10) is transformed to

$$R \mathbf{n} = \mathbf{S}^{-1} \mathbf{I}. \quad (11)$$

Due to the unit length of \mathbf{n} , R is computed as

$$R = \|\mathbf{S}^{-1} \mathbf{I}\|. \quad (12)$$

Given R , the unit surface normal vector \mathbf{n} can be computed

$$\mathbf{n} = \frac{1}{R} \mathbf{S}^{-1} \mathbf{I}. \quad (13)$$

For each pixel, the reflectance factor R and the three components of the unit surface normal vector \mathbf{n} are

² Klette et al. [8] the term R refers to $E\rho$, where E denotes the light source irradiance and ρ is in the true sense the surface albedo.

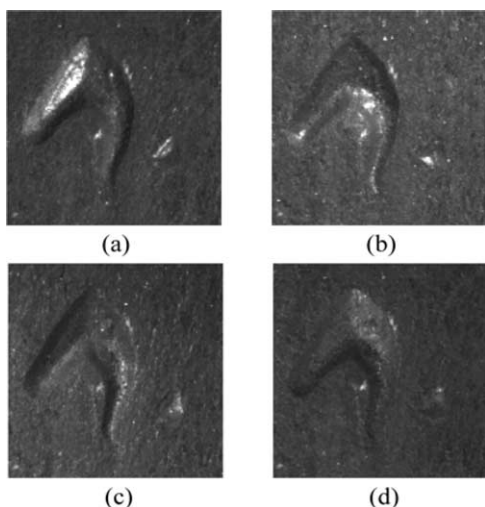


Fig. 9. Surface images with different illumination direction: (a) Illumination angle $\alpha = -22^\circ$, (b) $\alpha = 68^\circ$, (c) $\alpha = 158^\circ$, (d) $\alpha = 248^\circ$.

computed. The inverse of the light source matrix \mathbf{S} only exists, if the positions of the light sources do not lie on a straight line.

As mentioned above, photometric stereo is constrained to Lambertian reflecting surfaces. One method to overcome the specular problem of shiny surfaces is to add a fourth light source as suggested in Coleman and Jain [17]. Three images are necessary to uniquely determine the albedo and the surface normals. In the case of four images however, the pixels, which cover the specular reflection component show an elevated intensity value. Hence, these pixels are identified using the relative deviation of the four surface

reflectance factors R gained from each permutation of three intensity values. If for a pixel the relative deviation of R exceeds a certain threshold R_t , a specular contribution is present. Therefore, an accurate surface normal \mathbf{n} and albedo R are determined using the three intensity values which results in the smallest reflectance factor R . Otherwise, the surface normal vector and the albedo are computed by utilizing all four images. A limiting issue is that the specular regions from two or more light sources may not overlap.

Solomon and Ikeuchi [18] proposed a modification of the identification if a specular reflection is present in one of the four acquired images. They determine a statistically meaningful threshold based on the measured intensity variance of the camera.

Fig. 9 shows the four acquired images of a scale-covered steel block.

The specular reflections of the cavity and the intact surface are apparent. This fact restricts a successful application of surface inspection by means of intensity imaging (Section 2) of such surfaces. Both the surface normal vector \mathbf{n} and the surface albedo R of the images in Fig. 9 are computed according to the Eq. (12) and (13), where the specularities are removed by thresholding R as proposed in Coleman and Jain [17]. The recovered result of the surface orientation and the reflectance factor are shown in Fig. 10.

Often these results are already used for analysis of errors embedded in the surface by applying conventional rendering algorithms. Alternatively, the surface normal vector is used to recover the three-dimensional shape of the surface. Especially, one major advantage of

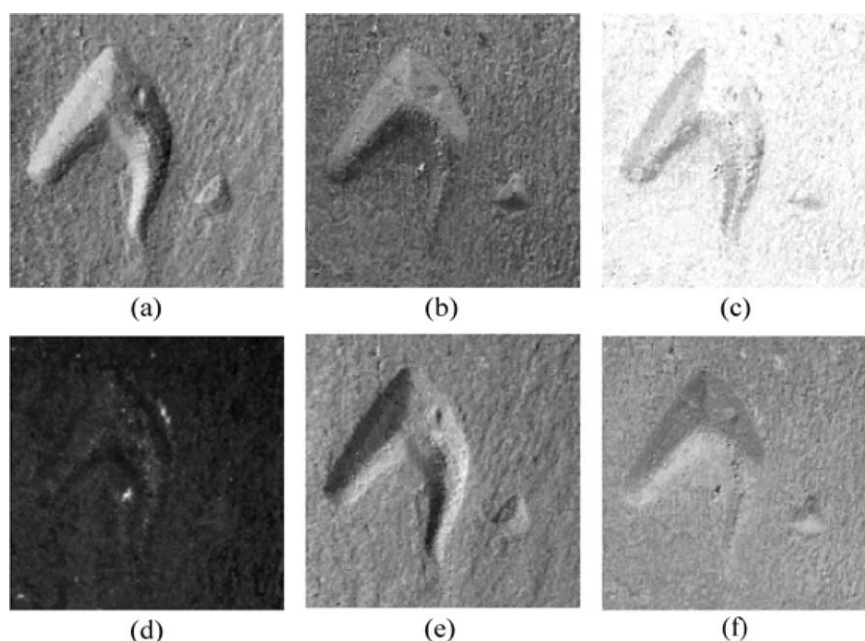


Fig. 10. Surface normal and surface albedo: (a) Surface normal component in x , (b) Surface normal component in y , (c) Surface normal component in z , (d) Surface albedo, (e) Gradient p , (f) Gradient q .

photometric stereo is the ability to discriminate between flaws which are affected by a change of the reflectance factor and defects which cause a change of the three-dimensional characteristic of the inspected surface.

Referring to images (e) and (f) in Fig. 10, the gradient space is a convenient method to represent surface orientation. The surface normal vector is expressed as

$$\mathbf{n} = [p \ q \ -1]^T, \quad (14)$$

where p and q are the gradients of the two-dimensional gradient space. Thus, p and q are derived from the components of the normal vector \mathbf{n}

$$p = -\frac{n_x}{n_z}, \quad (15)$$

$$q = -\frac{n_y}{n_z}. \quad (16)$$

The surface gradient gives the change of depth in the x and y direction.

3.2.1. Dealing with shadows

The issue of shadowing needs proper treatment in particular for shading based methods such as photometric stereo. Otherwise, this method produces incorrect results. Basically, there are several possibilities to overcome this problem:

- Deploying more than three light sources.
- Reduction of the angles between the illumination directions.
- Integration of other vision techniques.
- For regions which are illuminated by only two light sources two sets of surface normal vector solutions are available. The proper solution is selected by considering the boundary condition given by the shadow line [18].

3.2.2. Depth recovery from surface normals

This section reviews different methods for transforming the surface normals into depth data. A comparison of different algorithms is discussed in Schlüns and Klette [19,20].

Basically, they identify two different types of approaches, either local integration or global integration techniques.

Local integration. In local integration algorithms the depth is computed using the neighborhood of the treated pixel along a specified path. These algorithms are computationally efficient and simple to implement. Generally, a high accuracy of the data is necessary to achieve a reliable surface reconstruction. Otherwise, the error is accumulated and propagated along the integration path. In the following a short description of three different approaches is given.

1. The algorithm of Coleman and Jain [17] starts in the center of the image by choosing an arbitrary value for the surface depth. Afterwards, the depth along the row and the column intersecting the reference point is determined. Finally, the depth values are computed in each quadrant in column major order. Basically, in the first step only one and then two adjacent points to the currently treated point P are considered. The average tangent lines to P through the adjacent points are determined by using the surface normal vectors. The depth for P is obtained by averaging the results of the depth gained from the tangent lines from each of the two neighboring points. In the literature, this method is known as *two-point method*.
2. Healey and Jain [21], presented the *eight-point method*, an extension of the previously introduced algorithm. They consider eight points surrounding the point P for which the depth should be computed. A system of nine equations is solved for each set of nine points of the surface in row major order to obtain the relative depth of those nine points. These depth values are combined in an appropriate way, in order to achieve a consistent relative depth map for the entire surface.
3. Wu and Li [22], suggested a line-integration based approach for depth recovery from surface normal vectors. First, an arbitrary depth value is assigned to the reference point somewhere in the image. Then, the relative depth of a point is determined by computing the line integral (e.g. trapezoidal integration) with respect to the reference point. In their algorithm, they averaged the results achieved from integrating across multiple paths to reduce the propagated error in depth estimation.

Global integration. Global integration methods may treat the depth recovery as a minimization problem. Global techniques should be more robust with respect to noise [19] because the surface gradient data has a global influence on the solution.

Frankot and Chellappa [23] developed a surface depth reconstruction algorithm which is introduced in the following. The surface depth function $Z = Z(x, y)$ at each point in x and y should be recovered. For this function, the possibly non-integrable given gradient values $p(x, y)$ and $q(x, y)$ are approximated as a set of integrable surface slopes $\tilde{p}(x, y)$ and $\tilde{q}(x, y)$. To this end, Frankot and Chellappa [23] introduced the *integrability condition*

$$\frac{\partial \tilde{p}(x, y)}{\partial y} = \frac{\partial \tilde{q}(x, y)}{\partial x}. \quad (17)$$

Horn and Brooks [24] refer to this constraint of integrability as *smoothness* of the depth function which holds if the surface relief is twice differentiable independently of the order. This is the property of all C^2 surfaces, e.g. surfaces of polyhedral objects are excluded. Thus, the surface depth of any particular point is independent of the integration path.

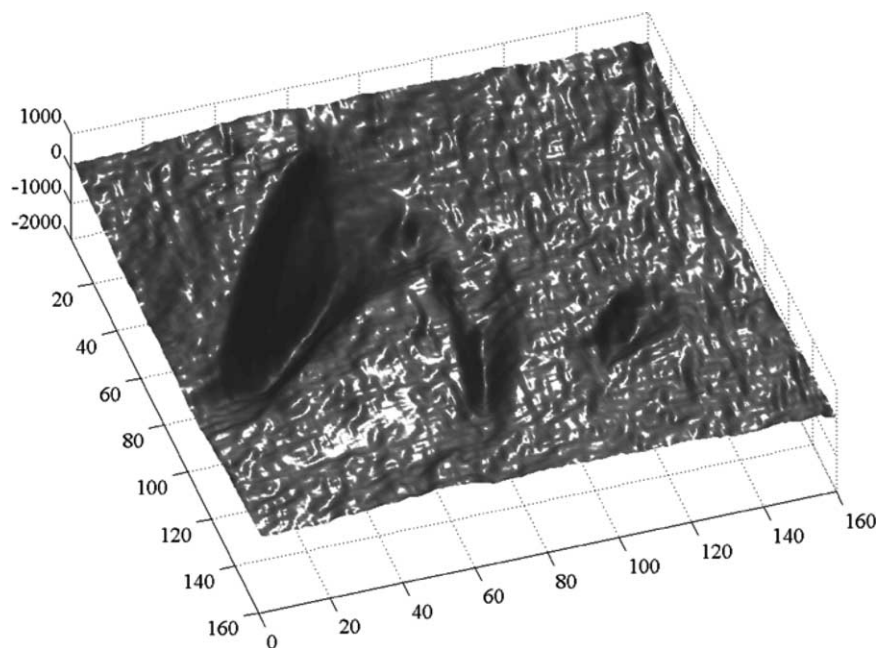


Fig. 11. 3D reconstruction from the surface normals.

Further, the function Z is chosen of the set of functions which satisfy the integrability condition so that the distance measure between given and ideal integrable gradients

$$d\{[\tilde{p}(x,y), \tilde{q}(x,y)], [p(x,y), q(x,y)]\} = \iint |p(x,y) - \tilde{p}(x,y)|^2 + |q(x,y) - \tilde{q}(x,y)|^2 dx dy \quad (18)$$

is minimized. The task of finding the minimum distance is simplified if the surface slopes can be represented by a finite set of basis functions which satisfy Eq. (17). The basis functions are assumed as Fourier functions and the stated minimization problem is solved [23] in the frequency domain $\Omega(\Omega = \{(u,v) : u = 2\pi x, v = 2\pi y\})$ if the values

$$\tilde{H}(u,v) = \frac{-jup(u,v) - jvq(u,v)}{u^2 + v^2} \quad (19)$$

are used as Fourier coefficients for $Z(u,v)$. $Z(u,v)$ denote the Fourier coefficients of $Z(x,y)$ in the frequency domain. The specified solution provides a minimal distance between the ideal and given gradient values. The depth map $Z(x,y)$ is acquired by using the inverse Fourier transform of $\tilde{H}(u,v)$. A more detailed description and the constraints of this global integration technique are given in Refs. [23,8].

According to Schlüns and Klette [19], the introduced global integration method is more robust against noise and consequently better for real scenes, especially curved objects.

The three-dimensional reconstruction from the surface normals (Fig. 10) using the global integration approach suggested in Ref. [23] is shown in Fig. 11.

There is a large variety of different approaches to depth recovery from surface normals in the literature, however,

their performance is restricted when the surface normals contain noise. It is assumed that there are mainly three reasons for the distortion in the reconstructed surface relief of Fig. 11.

1. Neglecting shadows which result from one or more light sources. Due to the arbitrary shapes of the defects a general valid illumination direction is difficult to determine. But also the use of a large number of light sources for avoiding shadows is irrelevant in practice.
2. Inter-reflections are not treated. It is assumed that each point on the surface is illuminated directly by one light source. This means that there is no mutual illumination between neighboring surface facets.
3. The specular components in certain image regions may not overlap within the consecutively acquired images. Therefore, most of the diffuse reflecting surface is acquired with low contrast, which results in a poor gray value resolution of these regions. This involves a large quantization error which causes noisy data.

4. Summary

Three imaging techniques with their optical arrangements for acquisition of the surface image for inspection applications of metallic objects have been presented. The most practical imaging techniques, such as intensity imaging and range imaging, are discussed with particular emphasis to their applicability and bottlenecks. One range imaging approach is based on light sectioning in conjunction with fast imaging sensors. The second one is photometric stereo, whereby the shape of the object is

gathered by analyzing the image intensities of a set of images obtained from the same viewpoint, while altering the illumination direction. The choice of the imaging technique is strongly connected to the characteristics of the flaws, the nature of the surface and the required spatial resolution.

References

- [1] Newman TS, Jain AK. A survey of automated visual inspection. *Comput Vision Image Underst* 1995;61(2):231–62.
- [2] Fernandes C, Platero C, Campoy P, Aracil R. Vision system for on-line surface inspection in aluminium casting process. In *IEEE Conference on Industrial Electronics, Control, Instrumentation and Automation*; 1993. p. 1854–59.
- [3] Vascotto M. High speed surface defect identification on steel strip. *Metall Plant Technol Int* 1996;4:70–3.
- [4] Stefani SA, Nagarajah CR, Willgross R. Surface inspection technique for continuously extruded cylindrical products. *Meas Sci Technol* 1999;10:N21–5.
- [5] Pernkopf F, O'Leary P. Visual inspection of machined metallic high-precision surfaces. *Spec Issue Appl Visual Inspect, Eurasip J Appl Signal Process* 2002;2002(7):667–78.
- [6] Pernkopf F, Pernkopf F, O'Leary P. Detection of surface defects on raw milled steel blocks using range imaging. In *IT&S/SPIE 14th Symposium Electronic Imaging*; 2002. p. 170–181.
- [7] Pernkopf F. Automatic visual inspection of metallic surfaces. PhD Thesis. University of Leoben; 2002.
- [8] Klette R, Schlüns K, Koschan A. *Computer vision: three-dimensional data from images*. Berlin: Springer; 1998.
- [9] Nayar SK, Ikeuchi K, Kanade T. Determining shape and reflectance of hybrid surfaces by photometric sampling. *IEEE Trans Rob Autom* 1990;6(4):418–31.
- [10] Naidu DK, Fisher RB. A comparative analysis of algorithms for determining the peak position of a stripe to sub-pixel accuracy. *Proceedings of the British Machine Vision Conference*; 1991. p. 217–25.
- [11] Leitner M, Ofner R, Pernkopf F. Comparison of algorithms for line detection in light-sectioning images. Technical report, Institute of Automation, University of Leoben; 2000.
- [12] IVP (Integrated Vision Products), Company. IVP Ranger SAH5 Product Information. URL: www.ivp.se.
- [13] Kanade T. *Three-dimensional machine vision*. Kluwer Academic Publishers; 1987.
- [14] Johannesson M. SIMD architectures for range and radar imaging. PhD. Thesis. University of Linköping; 1995.
- [15] Smith ML, Stamp RJ. Automated inspection of textured ceramic tiles. *Comput Ind* 2000;43:73–82.
- [16] Woodham RJ. Photometric method for determining surface orientation from multiple images. *Opti Engng* 1980;19(1):139–44.
- [17] Coleman EN, Jain R. Obtaining 3-dimensional shape of textured and specular surfaces using four-source photometry. *Comput Graphics Image Understanding* 1982;18:309–28.
- [18] Solomon F, Ikeuchi K. Extracting the shape and roughness of specular lobe objects using four light photometric stereo. *IEEE Trans Pattern Anal Mach Intell* 1996;18(4):449–54.
- [19] Schlüns K, Klette R. Local and global integration of discrete vector fields. In: Solina F, Kropatsch WG, Klette R, Bajcsy R, editors. *Advances in Computer Vision*. Berlin: Springer; 1997. p. 149–58.
- [20] Klette R, Schlüns K. Height data from gradient fields. In *machine vision applications, architectures, and systems integration V*, SPIE 2908; 1996. p. 204–15.
- [21] Healey G, Jain R. Depth recovery from surface normals. In *International Conference on Pattern Recognition, ICPR 1984*; 1984. p. 894–96.
- [22] Wu Z, Li L. A line-integration based method for depth recovery from surface normals. *Comput Vision, Graphics, Image Process* 1988;43: 53–66.
- [23] Frankot R, Chellappa R. A method for enforcing integrability in shape from shading algorithms. *IEEE Trans Pattern Anal Mach Intell* 1988; 10(4):439–51.
- [24] Horn BKP, Brooks MJ. The variational approach to shape from shading. *Comput Vision, Graphics, Image Process* 1986;33: 174–208.